Research Square

Preprints are preliminary reports that have not undergone peer review.
They should not be considered conclusive, used to inform clinical practice,
or referenced by the media as validated information.

Does PEO-PDA coating with Zoledronic acid have antitumor activity?

Konstantine Nadaraia

nadaraiakv@mail.ru

Institute of Chemistry FEB RAS

Mariya Mashurova

Institute of Chemistry FEB RAS

Maria Nadaraia

Institute of Chemistry FEB RAS

Vyacheslav Shandursky

Institute of Chemistry FEB RAS

Evgeniy Belov

Institute of Chemistry FEB RAS

Igor Imshinetskiy

Institute of Chemistry FEB RAS

Ivan Osmushko

Institute of Chemistry FEB RAS

Anastasia Golysheva

Institute of Chemistry FEB RAS

Ekaterina Pigul

Institute of Chemistry FEB RAS

Igor Manzhulo

A.V. Zhirmunsky National Scientific Center of Marine Biology Far Eastern Branch of the Russian Academy of Sciences

Arina Ponomarenko

A.V. Zhirmunsky National Scientific Center of Marine Biology Far Eastern Branch of the Russian Academy of Sciences

Dmitry Mashtalyar

Institute of Chemistry FEB RAS

Research Article

Keywords: Ti6Al4V titanium, implant, PEO coating, bisphosphonates, bioactive coatings

Posted Date: July 27th, 2026

DOI: https://doi.org/10.21203/rs.3.rs-10338711/v1

License: This work is licensed under a Creative Commons Attribution 4.0 International License.
Read Full License

Additional Declarations: No competing interests reported.

Abstract

The technologies for implant fabrication are improving every year. Currently, there is a significant demand for implants that not only exhibit high biocompatibility but also possess antibacterial, antiresorptive, and antitumor properties. In this study, we present a new method for creating implants based on the Ti6Al4V alloy, which surface was modified using plasma electrolytic oxidation followed by the formation of a polydopamine layer with bioactive substances. Vancomycin was used as the antibacterial component of the coating, while bisphosphonate (zoledronic acid) served as the antiresorptive agent. The presence of zoledronic acid and vancomycin in the surface layers was confirmed using X-ray photoelectron spectroscopy, scanning electron microscopy combined with energy-dispersive spectroscopy, and Raman spectroscopy. During MTS analysis, the culture medium extracted from the samples exhibited cytotoxic activity against human osteosarcoma cells (MNNG/HOS). The data obtained suggests the successful formation of a coating based on the titanium alloy and demonstrates the bioactive properties of the surface layers.

1 Introduction

Currently, there are no sufficiently reliable and generally accepted strategies for the use of endoprostheses made of materials other than titanium and its alloys in medicine. As a result, titanium remains the most used material for the manufacture of implants [1]. However, titanium is a foreign material for the human body, which leads to several problems associated with its use. One of the main problems is the need for additional processing to give the metal bioactive and biocompatible properties [2–5]. The formation of surface layers creates the opportunity to incorporate various bioactive substances with certain desired properties [2]. The introduction of biologically active agents into the implant surface is a promising approach for implant modification. The demand for implants that not only demonstrate biocompatibility with the patient's body but also reduce the risk of bacterial biofilm formation on the implant surface is growing [6]. Currently, a wide range of pathogens of nosocomial infections is known [7, 8]. Vancomycin is an antibiotic of last resort, effective against many pathogenic strains; thus, its inclusion in the coating composition significantly reduces the risk of inflammatory reactions and implant rejection [9–11].

In addition to antibacterial activity, it is important that implants have antiresorptive and/or antitumor properties to ensure effective use [12]. Therefore, the use of agents with such properties seems to be a rational solution. Zoledronic acid, a third-generation bisphosphonate, is part of the gold standard in the treatment of metabolic bone disorders such as osteoporosis, Paget's disease, tumor-induced hypercalcemia, and inflammation-related bone loss [13, 14]. In addition, there is evidence to support the antitumor activity of zoledronic acid [15, 16]. Thus, the introduction of zoledronic acid into the surface layer of implants may inhibit osteoclast proliferation, thereby promoting enhanced bone regeneration and accelerate patient recovery [17, 18].

The aim of this study was to develop and characterize a novel multifunctional bioactive coating on a Ti6Al4V alloy designed to impart antibacterial, antiresorptive and antitumor properties for potential orthopedic applications. This was achieved through sequential surface modification, including plasma electrolytic oxidation (PEO) to create a porous base layer, followed by immobilization of vancomycin and zoledronic acid in a polydopamine (PDA) matrix. To achieve this goal, the morphology and chemical composition of the coating were studied using scanning electron microscopy with energy-dispersive X-ray spectroscopy (SEM-EDS), X-ray photoelectron spectroscopy (XPS), and Raman spectroscopy. Its biological activity was also assessed by studying the coating's cytotoxicity toward murine NIH/3T3 fibroblasts and human osteosarcoma MNNG/HOS cells. The novelty of this study lies in the unique combination of PEO and PDA functionalization methods to create a dual drug delivery system on a titanium implant. Zoledronic acid and vancomycin were successfully co-immobilized on the surface of the PEO coating, as confirmed by XPS and Raman spectroscopy. The main result of the study was the demonstrated selective cytotoxicity: the released compounds exhibited pronounced antitumor activity against osteosarcoma, while weakening their effect on normal cells at higher dilutions, confirming the potential of the coating for use in bone cancer surgery to suppress tumor recurrence.

2 Materials and Methods

2.1 Samples

The base material for the manufacture of experimental samples was Ti6Al4V alloy. The samples were manufactured with dimensions of 8×8×1 mm^3. Before coating, the surfaces of the samples were standardized by sequential mechanical polishing using abrasive papers with a grain size decreasing to 3 μm. Then the samples were washed with distilled water and decreased in ethanol.

2.2 Coatings formation

The surface was functionalized using plasma electrolytic oxidation (PEO) [19]. The PEO process was performed in bipolar mode. In the first stage, the anodic phase was potentiodynamically increased from 50 to 400 V with a sweep rate of 1.75 V/s. In the second stage, the anodic phase was potentiastatically maintained at 400 V for 600 s. The cathodic phase was maintained at − 30 V throughout the process. Duty cycle was 0.5. Calcium acetate ($Ca(CH_3COO)_2$, 40 g/L) and calcium glycerylphosphate ($C_3H_7CaO_6P$, 30 g/L) was added to the electrolyte for formation Ca/P-reach surface layer. After completion of the process, the samples were washed with distilled water and dried at room temperature.

2.3 Composite coating formation

The subsequent polymerization of dopamine and simultaneous immobilization of zoledronic acid and vancomycin was carried out in an alkaline Tris-HCl buffer (pH 8.5). The concentrations of the components were as follows: dopamine chloride, 3 mg/ml; zoledronic acid, 0.03 mg/ml; vancomycin, 5 mg/ml (all Sigma Aldrich, USA, St. Louis, Missouri, analytical grade). The samples were immersed in the solution for 2 hours at room temperature with constant stirring at 200 rpm.

As a result, titanium samples with PEO coating and polydopamine (PDA) layer containing biologically active substances (zoledronic acid and vancomycin) were obtained. These samples are hereinafter referred as Ti-ZV. Samples without any coatings and only a PEO layer are referred as Ti and Ti-PEO, respectively.

2.4 Analysis of coatings composition and morphology

The surface morphology of the samples was examined using a Sigma scanning electron microscope (SEM, Carl Zeiss, Oberkochen, Germany). Cross-sectional analysis was performed using an EVO 40 scanning electron microscope (Carl Zeiss, Oberkochen, Germany) equipped with an X-ray energy dispersive spectroscopy (EDS) system for elemental analysis. Before SEM analysis, a thin conductive layer of chromium (100 nm) was sputtered onto the surface.

To study the chemical composition of the Ti-ZV surface, X-ray photoelectron spectroscopy (XPS) was used. The spectra were recorded using a Specs spectrometer (SPECS, Berlin, Germany) with a Phoibos-150 analyzer (radius 150 mm) and MgKα radiation (1253.6 eV) as an excitation source. All spectra were obtained at a constant analyzer transmission energy of 50 eV. Detailed analysis was performed on characteristic spectral regions with a step of 0.1 eV. In addition, Raman spectroscopy was used to characterize the composition of the hybrid coatings and PEO layers. Measurements were performed using an Alpha 500 Raman spectrometer (WITec, Ulm, Germany). A 532 nm laser with an output power of 20 mW was used for excitation. The spectra were obtained in the range of 0–3600 cm^{-1} for a total time of 60 min. Spectral analysis was performed using WITec Control software.

2.5 Wettability assay

The wettability of the resulting surface layers was measured by the sessile drop method on DCA100 drop shape analyzer (Krüss, Germany). In addition to distilled water, SBF served as a test liquid. Contact angle (CA) calculation was carried out using the Young–Laplace method [20].

The surface free energy (SFE) was calculated by the Owens-Wendt-Rabel-Kaelble method [21]. For the determination of CA, deionized water and CH_2I_2 (Sigma-Aldrich) were used since the surface tension of these two liquids was established with high accuracy [22]. The volume of the test liquid was 3 μl during all measurements. SFE was calculated according to Eq. 1:

$$\gamma_s = \gamma_s^d + \gamma_s^p$$

1

,

where γ_s is a SFE of solid phase, superscript indexes *d* and *p* are dispersive (Van-der-Waals interaction) and polar (dipole-dipole interactions, hydrogen bonds) components of the SFE, respectively.

γ_s^d and γ_s^p were determined graphically from the linearized Owens equation [21], in which the intersection with the ordinate axis corresponds to the root of the dispersed components, and the slope

of the straight line corresponds to the root of the polar components of the SFE of a solid phase (Eq. 2).

where γ_l is a liquid surface tension, *d* and *p* indexes are a dispersed and polar component of the liquid surface tension, respectively.

$$\gamma_l \frac{1+\cos(\theta)}{2\sqrt{\gamma_l^d}} = \sqrt{\gamma_s^d} + \sqrt{\gamma_s^p}\sqrt{\frac{\gamma_l^p}{\gamma_l^d}}\ ,$$

2

All the results were analyzed statistically and expressed as a mean ± standard deviation. For the calculated mathematical parameters, the error determined by the method of indirect measurements (considering the errors of the measured parameters). At least 5 samples were used for each experiment.

2.6 Corrosion tests

The tests were carried out in a three-electrode cell with a prepared sample as a working electrode and a platinized niobium mesh as a counter-electrode. As a reference electrode we have used a saturated calomel electrode (SCE). All studies conducted in simulated body fluid (SBF) [23] at the (37.0 ± 0.5) °C. The visible area of the working electrode was 1 cm^2. For open circuit potential (OCP) measurements and obtaining steady-state conditions each sample was exposed in electrolyte for 1 h. The last potential value was used during the electrochemical impedance spectroscopy (EIS). EIS were conducted from 10^{-2} to 10^5 Hz with a logarithmic sweep 7 points per decade. For modeling of EIS data equivalent electrical circuits (EEC) were used. And a constant phase element (CPE) was used instead of an ideal capacitance due to heterogeneity of studied surfaces [11].

Potentiodynamic polarization (PDP) of samples was conducted at a sweep rate of 1 mV/s in the range from E_C–0.25 V to E_C+3.00 V. The corrosion potential (E_C), corrosion current density (I_C), the slope of the cathodic and anodic polarization curves (β_c, β_a, respectively) were calculated using the Levenberg-Marquardt approach [19]. At least 3 samples were used for each measurement.

2.7 Cytotoxicity Assessment of Implants

To assess the cytotoxicity of substances released from the implants, an MTS assay was performed using the mouse fibroblasts line NIH/3T3 and human osteosarcoma cell line MNNG/HOS (the shared research facility "Vertebrate cell culture collection", Saint Petersburg, Russia). Cells were cultured in media previously prepared by incubation with Ti, Ti-PEO and Ti-ZV samples for 24 h. The resulting conditioned media were applied to the cells at serial dilutions: 1, 1/2, 1/4, and 1/8.

A comparative analysis was also performed using culture media collected after incubation with different types of implants: uncoated titanium samples, PEO-coated samples without bioactive agents, and

untreated control media. Cytotoxicity was assessed by co-culturing these media with NIH/3T3 and MNNG/HOS cells.

2.8 Statistics

All experiments were performed in triplicate (n = 3), and the results are presented as mean values ± standard deviation (SD). Statistical analysis was conducted using GraphPad Prism (version 10, GraphPad Software, San Diego, California, USA).

For comparisons between two groups, an unpaired two-tailed Student's t-test was applied. For multiple group comparisons, one-way analysis of variance (ANOVA) followed by Tukey's post hoc test was used. Differences were considered statistically significant at $p < 0.05$.

3 Results and Discussion

3.1 Morphology and composition of the samples

Scanning electron microscopy (SEM) analysis of the Ti-ZV sample (Fig. 1) reveals a typical morphology for this type of coating: a developed surface layer containing several through pores. The thickness of the coating varies from 25–30 to 50–55 μm. The distribution maps of elements over the coating thickness are presented in Fig. 1. The resulting layers mainly consist of titanium, calcium, phosphate and elements of organic compounds. Titanium and other alloy components, such as vanadium and aluminum, obviously are the main components of the substrate. The transfer of elements such as oxygen, silicon, calcium and phosphorus from electrolyte during PEO treatment explains the presence of these elements at the coating.

Additionally, energy dispersive spectroscopy (EDS) data indicate the presence of elements related to zoledronic acid, polydopamine (PDA) and vancomycin: C, N, O (Fig. 1), indirectly confirming the successful incorporation of these organic compounds into the coating [24]. Notably, nitrogen (N) and chlorine (Cl) are present not only in the coating but also in the substrate (Fig. 1); this is due to the water-soluble nature of vancomycin, which leads to partial leaching of the antibiotic during cross-section preparation.

As noted previously, X-ray photoelectron spectroscopy (XPS) was used to study the surface layer of the Ti-ZV sample. The obtained XPS spectra are shown in Fig. 2.

The N1s and P2p photoelectron signals serve as markers for the adsorption of zoledronic acid to the coating's surface. A strong N1s signal was anticipated and is clearly observed in Fig. 2. In addition to the N1s and P2p signals, other photoelectron signals include carbon (Fig. 2B, C1s, 285 eV) and oxygen (Fig. 2B, O1s, 531.7 eV) were detected.

Deconvolution of the high-resolution N1s spectrum revealed a peak at a binding energy of 400.2 eV, indicating that the nitrogen signal detected in the survey scan originates from the adsorption of both

bisphosphonate and vancomycin [25]. The P2p peak observed at 132.9 eV is attributed to phosphorus-containing groups in the bisphosphonate molecules, which further confirms the successful incorporation of zoledronic acid into the PEO coating.

The prominent peak at 400.2 eV is attributed to the NH_2 group in vancomycin. Additionally, an increased N/C ratio, as shown in Table 1 and Fig. 2B, and the presence of a Cl2p peak in the spectra of samples containing vancomycin confirm the presence of the antibiotic in the coating.

Upon binding vancomycin with PDA, the C1s spectra exhibit peaks at 285.0, 286.5, and 288.6 eV, corresponding to C–C/C–H, C–O/C–N, O–CO/C–Cl, and C = O, respectively (Fig. 2B, C1s), confirming the incorporation of vancomycin. Moreover, the peak at 530.5 eV is attributed to the C = O bond, the peak at 532.2 eV corresponds to the C–O–C (ether)/C–OH (hydroxyl) group, and the peak at 534.6 eV is characteristic of the O = C–O group, also confirming vancomycin binding (Fig. 2B, C1s).

The XPS N1s spectra for the Ti-ZV sample show three peaks at 398.2, 398.7, and 399.9 eV (Fig. 2B, N1s), characteristic of tertiary/aromatic amine, secondary, and primary amines, respectively. The higher percentage of secondary amine functionality confirms the polymerization of dopamine and the formation of PDA [26].

The Ti-ZV sample spectra also display peaks at 400.2 and 401.8 eV (Fig. 2B, N1s), corresponding to NH_2/amide nitrogen. The peak at 401.8 eV, associated with secondary amine/amide nitrogen, indicates the binding of the -NH_2 group of vancomycin with the quinone part of PDA.

Thus, XPS analysis confirms the successful formation of the desired types of bonds corresponding to the expected products (Fig. 2, Fig. S1).

The used bioactive substances as well as samples with coatings were also studied by Raman spectroscopy. Figure 3 shows the Raman spectra of zoledronic acid and vancomycin powders. Zoledronic acid was analyzed as a monohydrate. The characteristic Raman peaks correspond to those reported in the literature [16]. The band at 119 cm^{-1} is indicative of the crystalline structure of the substance. The peak at 249 cm^{-1} corresponds to C–C bond vibrations (Fig. 3, orange line). Peaks at 680 and 874 cm^{-1} are attributed to C–C and C = O bond vibrations within the zoledronic acid molecules, respectively. The band at 1400 cm^{-1} is associated with vibrations of the methylene group (CH_2) (Fig. 3, orange line). Peaks at 1004 and 1460 cm^{-1} are assigned to vibrations within the imidazole ring of the zoledronic acid molecule (Fig. 3, orange line). The high-frequency bands at 2974 and 3176 cm^{-1} correspond to C–H and –N–C– bond vibrations, respectively, within the zoledronic acid structure (Fig. 3, orange line).

The Raman spectrum of vancomycin exhibits characteristic peaks at 1236, 1328, 1599, and 1671 cm^{-1}, which are assigned to aliphatic C–C bonds, amino groups, cyclic C–C bonds, and carboxyl groups, respectively (Fig. 3A, yellow line). A prominent band at 2926 cm^{-1} corresponds to the methylene ($–CH_2–$) groups of vancomycin molecules (Fig. 3, yellow line) [27]. It should be noted that the concentration of

pure substances used in powder form for Raman spectroscopy was significantly higher than the concentrations used in the hybrid coatings formation.

Figure 3 also shows the Raman spectrum of the Ti-ZV sample. The characteristic peaks correspond to those described in the literature [28]. The peak at 152 cm^{-1} represents lattice vibrations in the crystal structure. The band at 331 cm^{-1} is associated with δ(CC) vibrations of aliphatic chains. A pronounced peak at 439 cm^{-1} corresponds to the stretching vibration of the Me–O group. The peak at 623 cm^{-1} is likely associated with υ(CC) vibrations of the aliphatic chain and may also indicate the presence of a υ(C–Cl) bond from vancomycin. The peak at 926 cm^{-1} is attributed to υ(C–O–C) bond vibrations, confirming the conjugation of vancomycin. Therefore, the Raman spectroscopic analysis supports the successful incorporation of the bioactive substances into the PEO coating.

Taken together, the analysis of the obtained data using various spectroscopic methods directly confirms the successful creation of a hybrid layer with antibacterial and antiresorptive components.

3.2 Wettability of coatings

An analysis of the results assessing the wettability of the samples indicates a significant influence of the method of surface modification on contact angle (CA) and, consequently, on surface free energy (SFE) (Fig. 4, Table 1). For the uncoated titanium sample, the contact angle is 63.7 ± 2.6° with distilled water and 52.9 ± 2.1° with SBF, indicating a hydrophilic surface character. Note that there is also an increase in SFE values (Fig. 4, Table 1). This behavior can be attributed to the native oxide film (TiO_2) bearing polar hydroxyl groups, as well as to the adsorption of carbonaceous contaminants from the atmosphere [29].

Surface modification by plasma electrolytic oxidation (Ti-PEO) sharply reduces the contact angle to 8.5 ± 0.5° for water and 7.3 ± 0.5° for SBF, rendering the surface superhydrophilic. This is accompanied by a marked increase in surface free energy (Fig. 4B). A comparable improvement in the wettability of titanium materials following PEO coating formation has been reported previously [21, 22]. Several factors account for this change in surface state. After the PEO layer forms the surface develops a well-defined porous relief, where the pores give rise to a capillary effect and, in turn, promote spreading of the droplet. In addition, given the variety of compounds present in the heterooxide layer, the likelihood of hydrogen bonding between these compounds and water molecules increases, which contributes to the rise in SFE (Fig. 4, Table 1).

Following modification of the PEO layer with polydopamine and zoledronate (Ti-ZV), the contact angle reaches 7.9 ± 0.4° for distilled water and 6.4 ± 0.4° for SBF, the highest degree of hydrophilicity among all the samples studied. The SFE of this sample is comparable to that of Ti-PEO 80.6 mJ/m^2, and the ratio of its dispersive and polar components remains essentially unchanged.

It is worth noting that, for every sample, the CA measured with SBF is lower than the corresponding value obtained with distilled water. This can be explained by the various cations and anions in SBF, which alter both the surface tension of the liquid and the nature of the interaction at the liquid/solid interface.

Taken together, the wettability results indicate that coating the titanium alloy surface provides a substantial improvement in surface hydrophilicity. The SFE values obtained for the modified samples are comparable to those reported in the literature as most favorable for osteoblast adhesion and proliferation 70 mJ/m² [30], which allows the developed coatings to be regarded as promising candidates for improving implant osteointegration.

Table 1

Calculated SFE and its dispersive and polar components ($mJ \cdot m^{-2}$) for different samples.

Sample	SFE, γ_s	Dispersive component, γ	Polar component, γ
Bare alloy	45,7 ± 2,0	32,5 ± 1,2	13,2 ± 1,6
Ti-PEO	80,5 ± 0,2	50,2 ± 0,1	30,3 ± 0,1
Ti-ZV	80,7 ± 0,1	50,4 ± 0,1	30,3 ± 0,1

3.3 Samples corrosion

OCP analysis indicates the influence of the method of surface treatment of the material on the dynamics of potential change, which is fully consistent with our previous work [19]. Thus, processing the base titanium samples increases the potential by approximately 1 V (Fig. 5A). This is explained by the formation of a ceramic-like PEO coating on the sample surface and the hindered penetration of solution ions to the titanium substrate. After the formation of the hybrid layer, changes occurred in the electrochemical behavior of the samples: a decrease in potential to ~ 0.1 V was observed (Fig. 5A). In this case, this decrease can be explained by the presence of hydrophilic components. When released from the coating surface, such hydrophilic components can interact with SBF ions, thereby slightly changing the potential.

The corrosion properties of the samples also vary depending on the method of modifying the surface of the material. The behavior of the bare titanium sample is typical for this material and was described in detail in our previous works [31, 19]. Thus, it can be noted that a shift in the current density is observed in the anodic region before reaching the potential values at which titanium passivation occurs (Fig. 4B). After applying coatings to the surface, a shift in the corrosion potential to a more positive region is observed (Fig. 4B, Table 2). Also, for these samples, there is no sharp shift in the potential in the anodic region (Fig. 5B). This is associated with the presence of a ceramic-like/hybrid layer, which significantly reduces the penetration of the corrosive environment to the substrate material.

Nevertheless, the analysis of the corrosion properties of the samples indicates an increase in the corrosion current density and a decrease in the polarization resistance after the formation of bioactive coatings (Table 2). We previously observed similar behavior on samples made of the TiAl6V4 titanium alloy [19]. This is directly related to the differences in the real and visible (1 cm^2) areas of working electrode. The PEO coating and, accordingly, hybrid coating have a significantly more developed surface

than the uncoated sample (Fig. 1). Accordingly, the contact area of the electrolyte with the working electrode is significantly larger for these samples than for the bare titanium sample. Thus, it can be concluded that the corrosion resistance of the coated samples is, at a minimum, not inferior to that of untreated titanium (considering the absence of any significant differences in the values of the corrosion parameters (Table 2) as well as shape of polarization curves (Fig. 5B).

Table 2
Corrosion properties (corrosion potential E_C, corrosion current density I_C, cathodic β_c and anodic β_a Tafel slops, polarization resistance R_P) for samples with different types of surface treatment.

Sample	E_C (V vs. SCE)	β_a (mV dec.$^{-1}$)	β_c (mV dec.$^{-1}$)	I_C (A cm^{-2})	R_P (Ω cm^2)
Ti	−0.46	180	186	7.8×10^{-8}	5.1×10^{5}
Ti-PEO	0.07	518	220	1.7×10^{-7}	3.9×10^{5}
Ti-ZV	−0.15	256	155	1.3×10^{-7}	3.2×10^{5}

The evaluation of the EIS results (Fig. 5C, Table 3) is in good agreement with the data obtained via PDP (Fig. 5B, Table 2). The highest impedance modulus value at low frequencies $|Z|_{f = 0.01\ Hz}$ was observed for the uncoated titanium alloy sample. While the values of this parameter for the PEO coating and the hybrid layer differ only slightly, they are lower than those for the uncoated titanium (Fig. 5C, Table 3). As with the PDP results, this is attributed to the significant difference between the actual and apparent surface areas of the samples (Fig. 1).

Analysis of the phase angle θ vs. frequency f dependence for the uncoated sample indicates the presence of a single time constant (a band with an extremum in the middle-frequency range; Fig. 5D). This time constant arises from the formation of a titanium oxide film on the sample surface, a characteristic feature of this metal and most of its alloys [19]. This film forms easily in oxygen-containing environments and is responsible for the corrosion resistance of titanium. We modeled the observed dependence using a single R-CPE circuit (Fig. 5E). In this case, the R and CPE components represent the charge-transfer resistance and the capacitance of the oxide film, respectively. Given the non-stoichiometric composition of the TixOy film, a CPE element was used instead of a pure capacitance.

Two time constants are clearly distinguishable in the Bode plots for the coated titanium samples (Fig. 5D). Despite the similarity of the presented plots, their physical interpretations differ. For the PEO coating, the first and second time constants arise from the outer porous layer (bands in the middle- and high-frequency range, Fig. 5D) and the inner thin sublayer (band in the low-frequency range, Fig. 5D), respectively. For the hybrid coating, the appearance of the first time constant (Fig. 5D) results from charge transfer through the porous outer layer of the coating, which is covered with thin polymer film. As with the PEO coating, the second time constant is attributed to the thin inner sublayer. Based on the

foregoing, an EEC comprising two R-CPE elements was used to model the electrochemical behavior of these samples (Fig. 5E).

The calculated values of the electrochemical system parameters (Table 3) are also of interest. An assessment of the presented data indicates that the application of a polymer layer containing vancomycin and zoledronate does not essentially alter the electrochemical parameters of the coatings. This is primarily due to the low thickness of the polymer film and the overall corrosion resistance of the materials under study. However, it is important to note the values of parameter n_2 (approximately 0.5, Table 3). Such values indicate the occurrence of diffusion processes. This diffusion may be attributed either to the presence of through-pores in the coating, allowing for charge transfer, and the composition of the inner sublayer, which consists mainly of titanium oxide.

Table 3
Calculated parameters of equivalent electrical circuits' elements ($|Z|_{f=0.01\ Hz}$ and R ($\Omega \cdot cm^2$), Q ($\Omega^{-1} \cdot cm^{-2} \cdot s^n$)) for samples with different types of surface treatment.

Sample	$\|Z\|_{f=0.01\ Hz}$	R_1	CPE_1		R_2	CPE_2	
			Q_1	n_1		Q_2	n_2
Ti	5.9×10^5	–	–	–	7.3×10^5	2.5×10^{-5}	0.92
Ti-PEO	1.7×10^5	5.0×10^3	2.8×10^{-6}	0.76	6.3×10^6	2.1×10^{-5}	0.48
Ti-ZV	1.2×10^5	8.4×10^3	3.5×10^{-6}	0.68	2.8×10^6	2.8×10^{-5}	0.46

Overall, it can be concluded that, despite a significant increase in wettability, neither the application of the PEO coating nor its subsequent modification with bioactive components results in any valuable change in the corrosion resistance of the titanium. Accordingly, combined with the presence of calcium-phosphate compounds on the surface, this indicates the high biocompatibility of the coatings and the effectiveness of proposed approach to modifying titanium implants.

3.4 Cytotoxicity Assessment of Implants

It was important to determine the toxic effect of the coating substances on normal cells of the body. Thus, when studying the medium obtained from Ti samples on a mouse fibroblast cell line, the absence of cytotoxic effect was revealed, which is confirmed by the absence of characteristic morphological changes. Interestingly, the coated samples not only exhibited no cytotoxicity but also increased cell proliferation compared to the positive control (Fig. 6). This can be explained by the following factors. First, the coatings have a developed morphology, which allows cells to better adhere to the surface (Fig. 1). Second, the coatings are hydrophilic [19] and, according to previously obtained data, possess optimal surface energy values for cell attachment [11].

The culture medium obtained by incubating Ti and Ti-PEO implants, when used on the MNNG/HOS cell line, without additional dilution and at a dilution of 2 times or more, does not demonstrate significant changes in the cytotoxic activity of the medium or the proliferative activity of the cells (Fig. 5), and does not cause any discernible changes in the morphology of osteosarcoma cells (MNNG/HOS). At some dilutions, an insignificant tendency towards an increase in the proliferative activity of human osteosarcoma cells (MNNG/HOS) is observed (Fig. 6). In addition, small foci of cell death are noticeable in the images obtained during the study of the culture media from the Ti-PEO samples, which, however, cannot be considered statistically significant. Thus, it can be concluded that titanium alloy samples with and without PEO coating do not have any antitumor effect.

When studying the culture medium obtained from Ti-ZV samples with the MNNG/HOS cell line, significant differences in the cell reaction were observed depending on the degree of medium dilution. The medium obtained from the samples was used in dilutions of 1, 1/2, 1/4, 1/8. Thus, the culture medium without additional dilution has pronounced cytotoxic activity, which confirms earlier studies on the cytotoxic activity of the studied drugs [16]. However, when the medium is diluted 2 and 4 times, the cytotoxic activity decreases in direct proportion and becomes statistically insignificant (Fig. 6). When the culture medium is diluted 8-fold, a significant increase in the proliferative activity of osteosarcoma cells is observed; this effect is presumably caused by a decrease in the concentration of the studied bioactive substances in the medium [32].

Thus, it can be concluded that the obtained hybrid coatings containing zoledronic acid exhibit cytotoxicity towards osteosarcoma cells and do not have any cytotoxicity against normal eukaryotic cells. This effect may be due to several factors. According to the paper [33–34], zoledronic acid exhibits cytotoxicity against osteosarcoma through multiple mechanisms: direct induction of apoptosis [35–36], suppression of osteoclastogenesis [37–38], antiangiogenesis [39], synergy with immunomodulation [40–41]. Additionally, immobilization of zoledronic acid on the implant surface allows its delivery to the area of direct contact between the implant and bone tissue. Taken together, these bioactive surfaces open up new treatment options for patients with bone trauma further complicated by osteosarcoma and/or bacterial infection.

4 Conclusion

In this study, a novel approach for fabricating titanium alloy-based implants with cytotoxic properties against osteosarcoma cells was presented. The developed coatings were formed via the immobilization of bioactive compounds (zoledronic acid and vancomycin) onto PDA/PEO-functionalized surfaces.

X-ray photoelectron spectroscopy (XPS) as well as EDS and Raman spectroscopy confirmed the successful incorporation of bioactive compounds into the PDA-PEO layer.

The MTS assay revealed cytotoxic activity of Ti-ZV implant eluates toward human osteosarcoma cells (MNNG/HOS) and most impotently absence of cytotoxicity against fibroblast cells (NIH/3T3).

These findings suggest that the developed surface modification enables the successful formation of functional coatings on titanium implants, with effective concentration of bioactive substances. Moreover, the observed cytotoxic effects of the coatings toward osteosarcoma cells highlight their potential for orthopedics applications.

Declarations

Acknowledgments

The formation of coatings, as well as SEM, EDS, XPS, Raman spectroscopy and cytotoxicity studies were supported by grant of the Russian Science Foundation No. 25-73-10044 https://rscf.ru/en/project/25-73-10044/.

The corrosion tests, as well as wettability assay were supported by grant of the Russian Science Foundation No. 23-13-00329П, https://rscf.ru/project/23-13-00329-П/.

Author contribution

Conceptualization, K.V.N. and D.V.M.; methodology, K.V.N.; validation, V.A.S. and M.A.N.; formal analysis, A.A.G.; investigation, I.M.I., A.A.G., E.S.P., V.A.S., M.V.M., M.A.N., E.A.B., I.S.O, I.V.M. and A.I.P.; resources, I.M.I. and K.V.N.; data curation, K.V.N.; writing - original draft preparation, I.V.M., K.V.N., A.A.G., M.V.M. and V.A.S.; writing - review and editing, K.V.N. and D.V.M.; visualization, M.V.M., A.I.P. and V.A.S.; supervision, K.V.N. and D.V.M.; project administration, K.V.N. and D.V.M.; funding acquisition, K.V.N. and D.V.M.

Data availability

The data that support the findings of this study are available from the corresponding author upon reasonable request.

Declarations

8.1 Conflict of interest

The authors declare that they have no conflict of interest.

8.2 Ethics Approval

This study did not involve human participants or animals, and no ethical approval was required. All research procedures adhered to relevant ethical guidelines and best practices for non-human and non-animal research. The authors declare that

This manuscript is original, has not been published before, and is not currently being considered for publication elsewhere. All authors agreed with the final version of this manuscript and with the current submission.

References

1. K.T. Kim, M.Y. Eo, General review of titanium toxicity. Int. J. Implant Dent. **5**, 10 (2019). https://doi.org/10.1186/s40729-019-0162-x
2. R.C.S. Silva, A. Agrelli, Titanium Dental Implants: An Overview of Applied Nanobiotechnology to Improve Biocompatibility and Prevent Infections. Materials. **15**, 3150 (2022). https://doi.org/10.3390/ma15093150
3. A. Bandyopadhyay, I. Mitra, A review of titanium for next generation of metallic implants. Prog Mater. Sci. **133**, 101053 (2023). https://doi.org/10.1016/j.pmatsci.2022.101053
4. M. Sarraf, E.R. Ghomi, A state-of-the-art review of the fabrication and characteristics of titanium and its alloys for biomedical applications. Biodes Manuf. **5**, 371–395 (2022). https://doi.org/10.1007/s42242-021-00170-3
5. J. Stepanovska, R. Matejka, Treatments for enhancing the biocompatibility of titanium implants. Biomedical Papers. **164**, 23–33 (2020). https://doi.org/10.5507/bp.2019.062
6. A. Shahid, B. Aslam, The prospects of antimicrobial coated medical implants. J. Appl. Biomater. Funct. Mater. **19**, 228080002110403 (2021). https://doi.org/10.1177/22808000211040304
7. H.Y. Ahmadabadi, K. Yu, Surface modification approaches for prevention of implant associated infections. Colloids Surf. B Biointerfaces. **193**, 111116 (2020). https://doi.org/10.1016/j.colsurfb.2020.111116
8. J. Sahoo, S. Sarkhel, Nanomaterial-Based Antimicrobial Coating for Biomedical Implants: New Age Solution for Biofilm-Associated Infections. ACS Omega. **7**, 45962–45980 (2022). https://doi.org/10.1021/acsomega.2c06211
9. C.J. Rajkovic, J.A. Tracz, Synthesis and evaluation of a novel vancomycin-infused, biomimetic bone graft using a rat model of spinal implant-associated infection. North. Am. Spine Soc. J. (NASSJ). **18**, 100323 (2024). https://doi.org/10.1016/j.xnsj.2024.100323
10. K.V. Nadaraia, D.V. Mashtalyar, Antibacterial HA-coatings on bioresorbable Mg alloy. J. Magnesium Alloys. **12**(5) (2024). https://doi.org/10.1016/j.jma.2024.05.006
11. M.A. Piatkova, K.V. Nadaraia, Hybrid surface layers with antibacterial and anti-inflammatory activity for implants materials. J. Magnesium Alloys. **13**(5) (2025). https://doi.org/10.1016/j.jma.2025.04.014
12. G. Tan, J. Xu, Antibacterial and Anti-Inflammatory Coating Materials for Orthopedic Implants: A Review. Coatings. **11**(11), 1401 (2021). https://doi.org/10.3390/coatings11111401
13. X. Shi, Y. Wang, Enhancing Alendronate Release from a Novel PLGA/Hydroxyapatite Microspheric System for Bone Repairing Applications. Pharm. Res. **26**, 422–430 (2009). https://doi.org/10.1007/s11095-008-9759-0
14. G.A. Rodan, MECHANISMS OF ACTION OF BISPHOSPHONATES. Annu. Rev. Pharmacol. Toxicol. **38**, 375–388 (1998). https://doi.org/10.1146/annurev.pharmtox.38.1.375

15. L. Wang, D. Fang, Various pathways of zoledronic acid against osteoclasts and bone cancer metastasis: a brief review. BMC Cancer. **20**, 1059 (2020). https://doi.org/10.1186/s12885-020-07568-9
16. G.Q. Vélez, S. Carmona-Sarabia, High affinity zoledronate-based metal complex nanocrystals to potentially treat osteolytic metastases. Mater. Adv. **3**, 3251–3266 (2022). https://doi.org/10.1039/D1MA01127. H? urlappend=%3Futm_source%3Dresearchgate.net%26utm_medium%3Darticle
17. I.R. Orriss, M.L. Key, Inhibition of osteoblast function in vitro by aminobisphosphonates. J. Cell. Biochem. **106**, 109–118 (2009). https://doi.org/10.1002/jcb.21983
18. von F. Knoch, C. Jaquiery, Effects of bisphosphonates on proliferation and osteoblast differentiation of human bone marrow stromal cells. Biomaterials. **26**, 6941–6949 (2005). https://doi.org/10.1016/j.biomaterials.2005.04.059
19. K.V. Nadaraia, D.V. Mashtalyar, A first look at the formation of PEO-PDA coatings on 3D titanium. ChemPhysMater 3(4), 451–461 (2024). https://doi.org/10.1016/j.chphma.2024.07.002
20. R. Finn, The contact angle in capillarity. Phys. Fluids. **18**(4) (2006). https://doi.org/10.1063/1.2185655
21. D.K. Owens, R.C. Wendt, Estimation of the surface free energy of polymers. J. Appl. Polym. Sci. **13**(8), 1741–1747 (1969). https://doi.org/10.1002/app.1969.070130815
22. J.J. Jasper, The surface tension of pure liquid compounds. J. Phys. Chem. Ref. Data. **1**(4), 841–1010 (1972). https://doi.org/10.1063/1.3253106
23. T. Kokubo, H. Takadama, How useful is SBF in predicting in vivo bone bioactivity? Biomaterials. **27**(15), 2907–2915 (2006). https://doi.org/10.1016/j.biomaterials.2006.01.017
24. Y. Zou, X. Chen, Regulating the absorption spectrum of polydopamine. Sci. Adv. **6**(36) (2020). https://doi.org/10.1126/sciadv.abb4696
25. S. Chen, P. Wan, Facile fabrication of the zoledronate-incorporated coating on magnesium alloy for orthopaedic implants. J. Orthop. Translat. **22**, 2–6 (2020). https://doi.org/10.1016/j.jot.2019.09.007
26. R.A. Zangmeister, T.A. Morris, Characterization of Polydopamine Thin Films Deposited at Short Times by Autoxidation of Dopamine. Langmuir. **29**, 8619–8628 (2013). https://doi.org/10.1021/la400587j
27. R. Aerts, W. Herrebout, Raman optical activity of the antibiotic vancomycin bound to its biological target. J. Raman Spectrosc. **53**(7), 1220–1226 (2022). https://doi.org/10.1002/jrs.6347
28. HORIBA, *Raman Spectroscopy for Analysis and Monitoring*. Raman Bands
29. Kido, D., Komatsu, K., Suzumura, T., Matsuura, T., Cheng, J., Kim, J., … Ogawa, T.(2023). Influence of surface contaminants and hydrocarbon pellicle on the results of wettability measurements of titanium. International Journal of Molecular Sciences,24(19), 14688. https://doi.org/10.3390/ijms241914688

30. B. Majhy, P. Priyadarshini, Effect of surface energy and roughness on cell adhesion and growth–facile surface modification for enhanced cell culture. RSC Adv. **11**(25), 15467–15476 (2021). https://doi.org/10.1039/d1ra02402g
31. D.V. Mashtalyar, K.V. Nadaraia, Composite coatings formed on Ti by PEO and fluoropolymer treatment. Appl. Surf. Sci. **536**, 147976 (2021). https://doi.org/10.1016/j.apsusc.2020.147976
32. J. Braun, S. Eckes, Toxic Effect of Vancomycin on Viability and Functionality of Different Cells Involved in Tissue Regeneration. Antibiotics. **9**, 238 (2020). https://doi.org/10.3390/antibiotics9050238
33. P. Clezardin, Potential anticancer properties of bisphosphonates: insights from preclinical studies. Anti Cancer Agents Med. Chem. **12**(2), 102–113 (2012). https://doi.org/10.2174/187152012799014977
34. G. Cai, D. Aitken, Effect of intravenous Zoledronic acid on Tibiofemoral cartilage volume among patients with knee osteoarthritis with bone marrow lesions: a randomized clinical trial. Jama. **323**(15), 1456–1466 (2020). https://doi.org/10.1001/jama.2020.2938
35. P. Li, H. Yang, Experimental study on inhibitory effect of zoledronic acid on the action style of the osteoclast. Sheng wu yi xue gong cheng xue za zhi 34(1), 78–82 (2017). https://doi.org/10.7507/1001-5515.201601041
36. X. Li, W. Sun, Clomipramine causes osteoporosis by promoting osteoclastogenesis via E3 ligase Itch, which is prevented by Zoledronic acid. Sci. Rep. **7**, 41358 (2017). https://doi.org/10.1038/srep41358
37. H. Peng, Y. Sohara, The Activity of Zoledronic Acid on Neuroblastoma Bone Metastasis Involves Inhibition of Osteoclasts and Tumor Cell Survival and Proliferation. Cancer Res. **67**(19), 9346–9355 (2007). https://doi.org/10.1158/0008-5472.can-06-4508
38. T. Hiraga, P.J. Williams, Zoledronic Acid Inhibits Visceral Metastases in the 4T1/luc Mouse Breast Cancer Model. Clin. Cancer Res. **10**(13), 4559–4567 (2004). https://doi.org/10.1158/1078-0432.ccr-03-0325
39. S. Gao, G. Zheng, Zoledronate suppressed angiogenesis and osteogenesis by inhibiting osteoclasts formation and secretion of PDGF-BB. PLOS ONE. **12**(6), e0179248 (2017). https://doi.org/10.1371/journal.pone.0179248
40. K. Morii, Y. Aoyama, Synergistic Anti-Tumor Effects of Zoledronic Acid and Radiotherapy against Metastatic Hepatocellular Carcinoma. Intern. Med. **54**(20), 2609–2613 (2015). https://doi.org/10.2169/internalmedicine.54.4430
41. Y. Yamakawa, H. Tazawa, Role of zoledronic acid in oncolytic virotherapy: Promotion of antitumor effect and prevention of bone destruction. Cancer Sci. **108**(9), 1870–1880 (2017). https://doi.org/10.1111/cas.13316

Figures

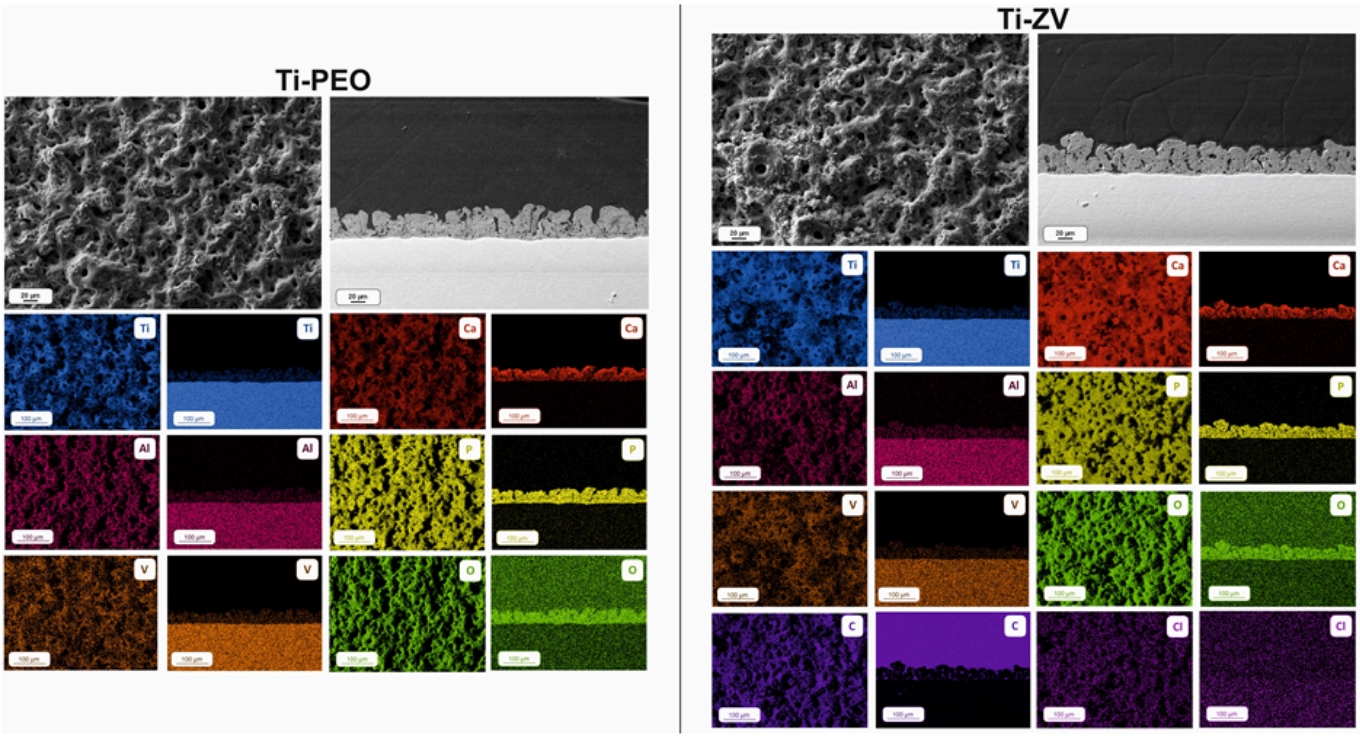


Figure 1

SEM images with EDS maps of the Ti-PEO and Ti-ZV.

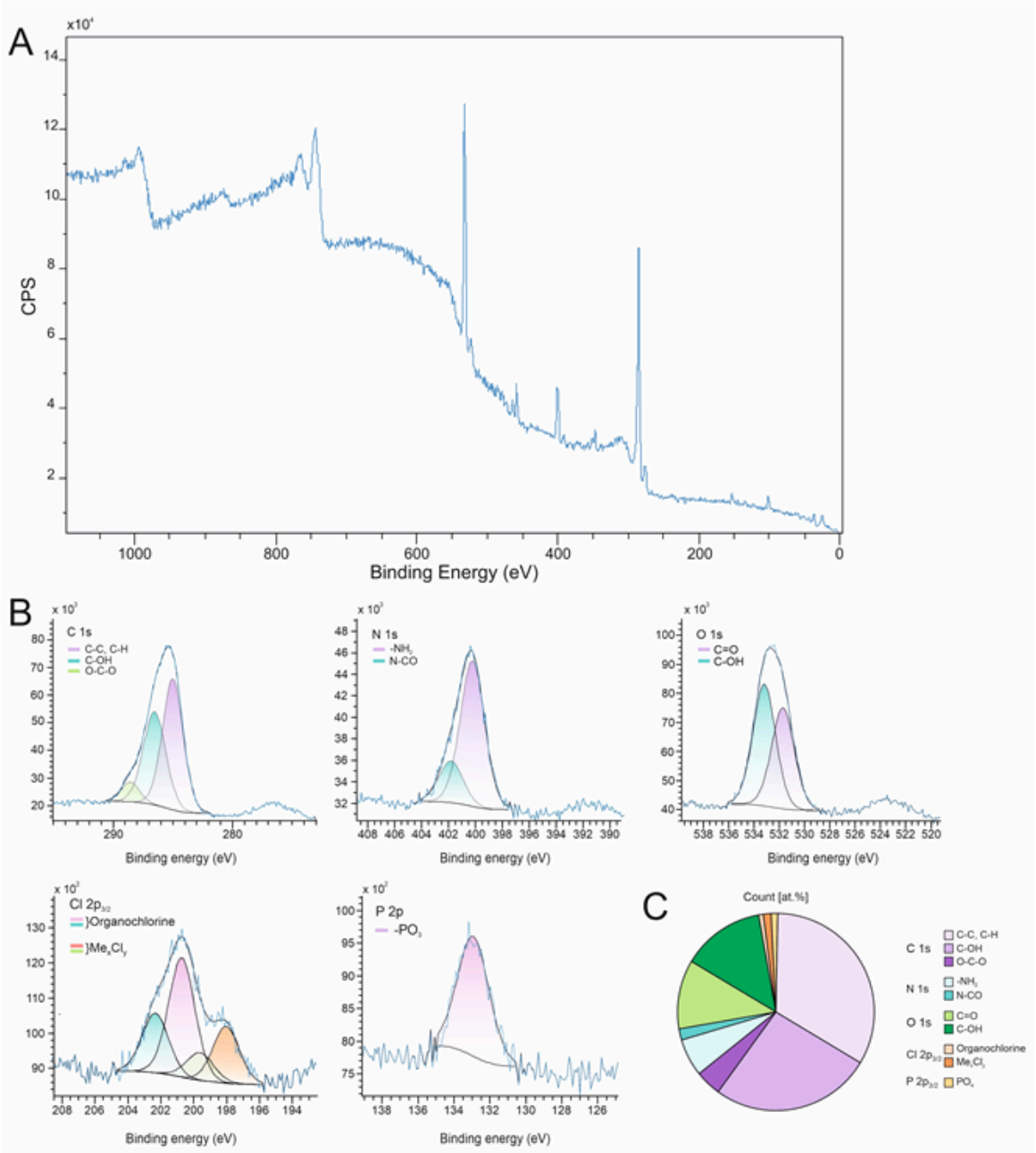


Figure 2

XPS survey (A), high-resolution XPS spectra of Ti-ZV coating (B) and concentration of the main elements in the coating (C).

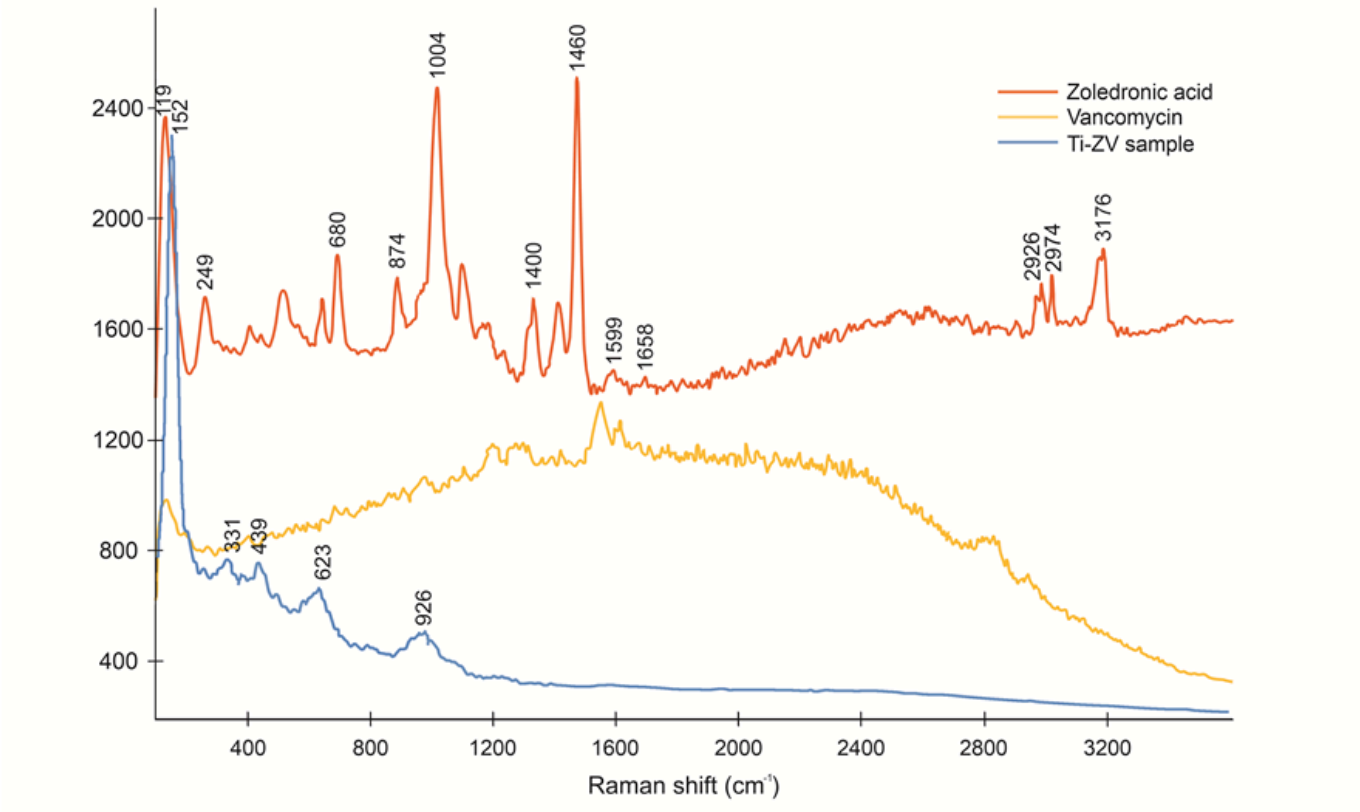


Figure 3

Raman spectra of bioactive substances and Ti-ZV sample.

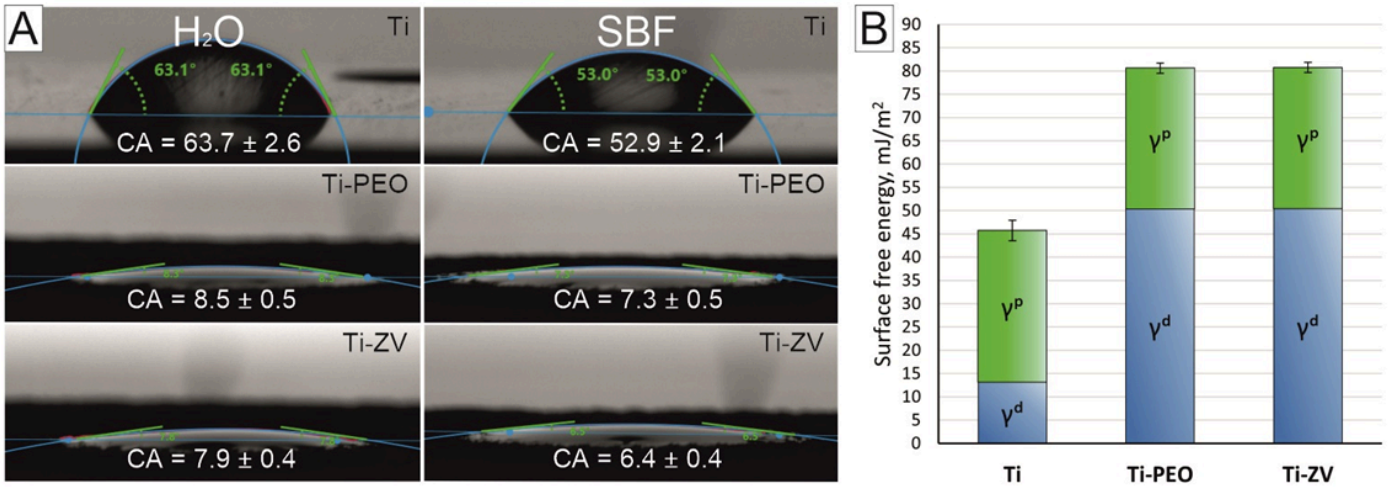


Figure 4

Wettability and surface free energy of the studied samples: (A) contact angles for distilled water (H_2O) and SBF; (B) SFE values resolved into dispersive (γ) and polar (γ) components.

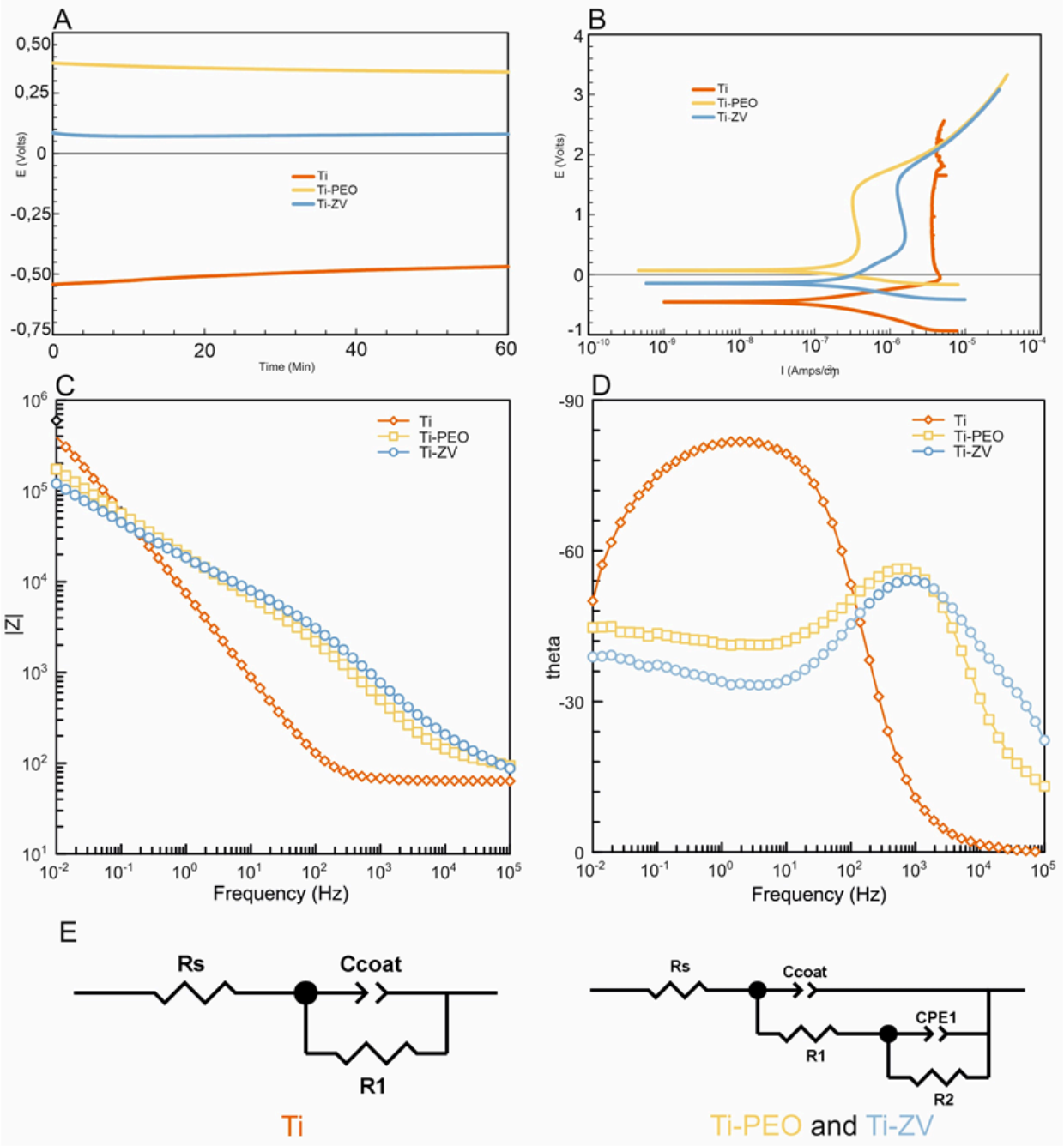


Figure 5

OCP vs. time for 60 min of exposure in SBF (A), polarization curves (B), and Bode plots (dependence of impedance modulus |Z| (C) and phase angle θ (D) on frequency) for Ti, Ti-PEO, Ti-PEO-ZV samples. The symbols are experimental data; the lines are the fitting curves. EEC used to simulate the charge transfer process at the sample / electrolyte interface (E).

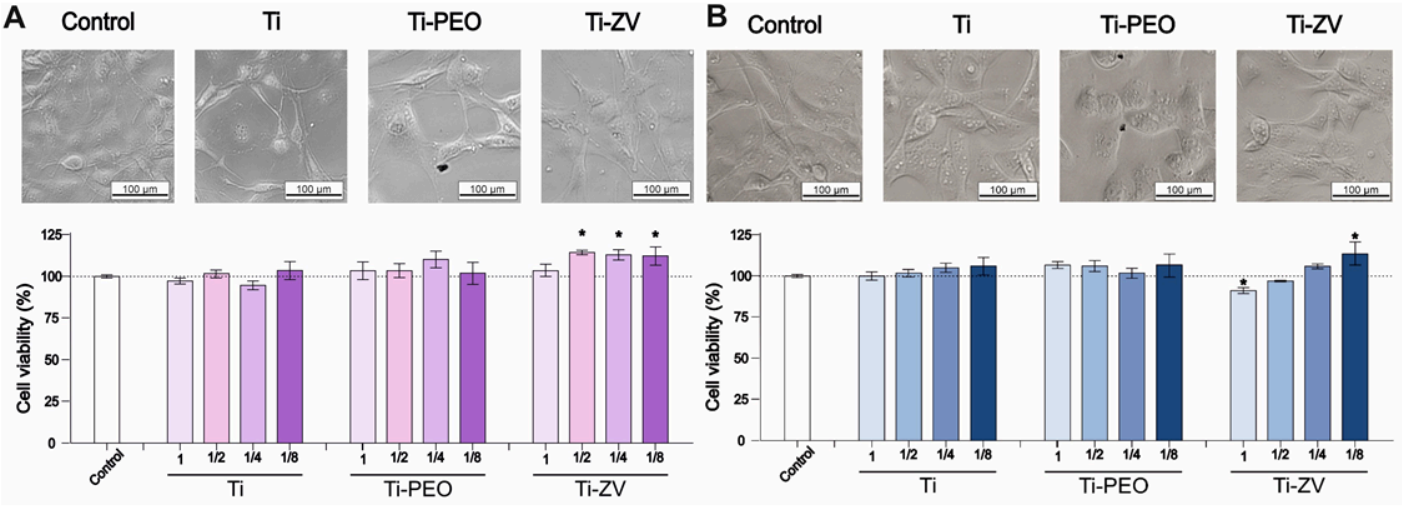


Figure 6

Cytotoxic activity of the culture medium after incubation with implants in co-culture with mouse fibroblast cells (NIH/3T3) (A) and with human osteosarcoma cells (MNNG/HOS) (B). *Significant differences between the control group and different types of implants. Data are presented as mean±standard error of the mean, $P<0.05$, $n=9$.